

ARTICLE

Received 11 Mar 2013 | Accepted 3 Jul 2013 | Published 1 Aug 2013

DOI: 10.1038/ncomms3251

OPEN

Angiomotin prevents pluripotent lineage differentiation in mouse embryos via Hippo pathway-dependent and -independent mechanisms

Chuen Yan Leung^{1,2} & Magdalena Zernicka-Goetz^{1,2}

Cell identity is specified in the early mammalian embryo by the generation of precursors for two cell lineages: the pluripotent inner cell mass and differentiating trophectoderm. Here we identify Angiomotin as a key regulator of this process. We show that the loss of Angiomotin, together with Angiomotin-like 2, leads to differentiation of inner cell mass cells and compromised peri-implantation development. We show that Angiomotin regulates localization of Yap, and Yap-binding motifs are required for full activity of Angiomotin. Importantly, we also show that Angiomotin function can compensate for the absence of Lats1/2 kinases, indicating the ability of Angiomotin to bypass the classical Hippo pathway for Yap regulation. In polarized outside cells, Angiomotin localizes apically, pointing to the importance of cell polarity in regulating Yap to promote differentiation. We propose that both Hippo pathway-dependent and Hippo pathway-independent mechanisms regulate Yap localization to set apart pluripotent and differentiated lineages in the pre-implantation mouse embryo.

¹The Wellcome Trust/Cancer Research UK Gurdon Institute, the Henry Wellcome Building of Cancer and Developmental Biology, University of Cambridge, Tennis Court Road, Cambridge CB2 1QN, UK. ²Department of Physiology, Development and Neuroscience, University of Cambridge, Downing Street, Cambridge CB2 3EG, UK. Correspondence and requests for materials should be addressed to M.Z.G. (email: mz205@cam.ac.uk).

As development progresses, cell identity must be correctly specified. In early mammalian development, three cell types have to be set apart by the blastocyst stage: epiblast, which will give rise to the embryo proper, trophectoderm (TE) and primitive endoderm (PE), which will provide the extra-embryonic structures such as the placenta and yolk sac. Specifying these three cell lineages is mediated through three waves of asymmetric cell divisions that start at the eight-cell stage and generate nonpolar inside and polar outside cells^{1,2}. Inside cells constitute the so-called inner cell mass (ICM) and will develop further as either the pluripotent epiblast or the PE, largely depending on whether an inside cell is generated by the first, second or third wave of asymmetric division^{3,4}. Outside cells will progressively differentiate into TE. Thus, inside and outside cells are progenitors for pluripotent ICM and TE lineages, respectively.

Three lines of evidence indicate that regulation of expression of the transcription factor *Cdx2* is particularly crucial to initiate diversification of ICM and TE lineages^{5–8}. First, *Cdx2* is the first transcription factor identified thus far whose expression becomes restricted to the outside cells as soon as they form⁶, whereas pluripotency factors are initially expressed in both inside and outside cells. Second, *Cdx2* downregulation leads to the upregulation of pluripotency genes in outside cells and, consequently, inhibition of TE formation and developmental arrest^{5,6}. Finally, experimental upregulation of *Cdx2* in inside cells prevents pluripotency of the ICM⁸.

The differential expression of *Cdx2* between ICM and TE progenitor cells is brought about along two major routes. We recently found that one of these routes involves asymmetric, apical localization of *Cdx2* mRNA that results in outside cells inheriting more *Cdx2* mRNA than inside cells upon asymmetric cell division^{6,8}. Accordingly, preventing the asymmetric localization and inheritance of *Cdx2* mRNA leads to the accumulation of *Cdx2* protein in inside cells and, consequently, inhibition of pluripotency genes such as *Nanog*⁸. In a second route, transcriptional control is achieved through localization of a transcriptional co-activator Yap, which permits Tead4-mediated transcription of *Cdx2* (ref. 9). In the polarized outside cells, Yap is nuclear, whereas in inside non-polarized cells Yap is cytoplasmic. This localization of Yap in mouse embryos is surprising because in other model systems Yap is retained in the cytoplasm of polarized cells, through the activity of apically associated proteins such as Crumbs, Merlin, Expanded and Angiomotin (Amot)^{10–13}. This raises the question of whether, and if so how, cell polarity

might be involved in regulation of Yap localization in the mouse embryo. To resolve this conundrum, it has been proposed that the differential localization of Yap in the mouse is achieved through differential Hippo signalling due to differences in the cell–cell contacts between the inside and outside cells⁹. However, whether there might be an alternative mechanism involved in controlling Yap localization to regulate expression of differentiation genes such as *Cdx2* and lineage segregation in mouse development has remained unknown.

Here we wished to elucidate further the mechanisms underlying the regulation of *Cdx2* expression and the potential role of cell polarity in affecting localization of Yap to control this process. To this end, we chose to follow the role of Amot, a protein known to bind to both tight-junction proteins and also to Yap/Taz^{11–17}. Amot is known to have an important role in a variety of developmental processes^{18,19}, but any role for Amot in the pre-implantation embryo has been unknown. Our results indicate that cell polarity contributes to directing the localization of Amot and of Yap in early mouse development. Importantly, Yap localization and therefore *Cdx2* expression is regulated not only through a Hippo pathway-dependent mechanism but also through a Hippo pathway-independent mechanism.

Results

Differential expression of Amot in ICM and TE precursors. To determine the potential function of Amot in regulating cell-lineage specification in mouse embryos, we first examined its expression throughout pre-implantation development. Interrogation of our previously generated genome-wide microarray data set²⁰ indicated that *Amot* expression rises from the four-cell stage to peak at the early blastocyst stage. This prompted us to analyse the localization pattern of Amot protein, using an antibody that detects the C-terminal part of both p130 and p80 isoforms (Fig. 1). We were able to detect Amot protein from the late eight-cell stage onwards when it becomes localized to the membrane, consistent with Amot being a membrane-associated protein²¹. However, when progenitors of the ICM and TE lineages become set apart, at the 8- to 16-cell transition, Amot becomes localized throughout the membrane in the inside cells, whereas in outside cells it is restricted to the apical domain (Fig. 1). As development progresses, Amot becomes highly expressed in the ICM but barely detectable in the TE (Fig. 1). These results indicate that Amot becomes expressed and localized

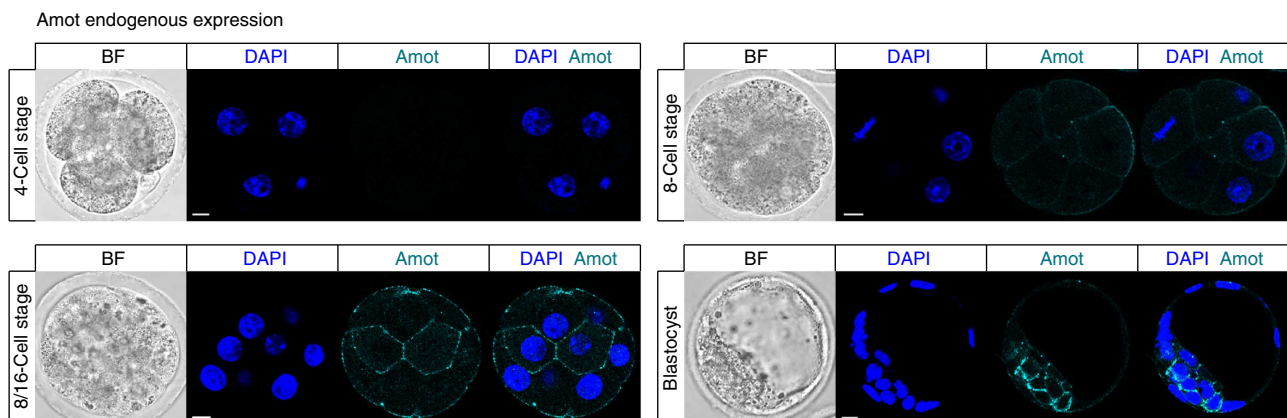


Figure 1 | Amot expression and localization in pre-implantation embryos. Immunofluorescent confocal images of Amot. Amot is first detected at the compacted eight-cell stage, where it is localized to the membrane ($N=16$). At the 8- to 16-cell transition, Amot is localized apically in the outside cells and throughout the membrane of the inside cells ($N=12$). By the blastocyst stage, Amot is much more abundant in the ICM compared with the TE ($N=18$). Weak Amot staining can be seen on the apical domain of TE cells. Yellow areas and dotted lines mark inside cells. Scale bar, 10 μm .

differentially between the progenitors of the pluripotent ICM and the differentiating TE lineages.

Amot is required to prevent differentiation of the ICM. To determine the role of Amot, we used RNA interference (RNAi) to specifically downregulate its expression from the zygote stage²². Amot small interfering RNAs (siRNAs) were injected into the zygote, together with Ruby mRNA as a marker of successful injection, and developmental progression was compared with embryos injected with control siRNA (Fig. 2a). Three different siRNAs for Amot were injected and the siRNA resulting in the highest knockdown efficiency ($79.1 \pm 4\%$ by qRT-PCR) (Fig. 2c) was used in subsequent experiments. We also confirmed Amot depletion at the protein level (Fig. 2a). Amot depletion did not prevent blastocyst formation (Fig. 2a) and did not affect total cell number (Fig. 2b). However, we found that Cdx2, critical for TE differentiation, was detectable not only in the TE but also within the ICM in Amot-RNAi embryos (Fig. 2a). Overall, $61.8 \pm 5\%$ of total ICM cells in Amot-RNAi blastocysts were clearly expressing Cdx2, as compared with $5.0 \pm 2\%$ in control embryos (Fig. 2b). As we observed that the absence of Amot leads to Cdx2 expression in the ICM, we examined the localization of the co-activator of Cdx2 expression, Yap⁹. We found Yap to be localized to the nuclei of ICM cells upon Amot-RNAi (Fig. 2a). Amot depletion also led to the expression of other TE-marker genes such as Eomes and Ck-8 (Troma-1) in the ICM (Fig. 2a). The use of an siRNA control, together with rescue experiments (described later), indicate that the Amot-RNAi phenotype is specific and not an artefact of either microinjection or off-target effects.

We next wished to determine the consequences of Amot-RNAi on pluripotency factors. qRT-PCR of Amot-RNAi blastocysts revealed that the transcript levels of Oct4, Nanog and Sox2 were significantly reduced to $38.5 \pm 11\%$, $29.8 \pm 2\%$ and $17.4 \pm 5\%$, respectively ($P < 0.05$, Student's *t*-test) (Fig. 2c), although Oct4 and Nanog proteins were still detectable (Fig. 2a). In contrast, and in agreement with our earlier analyses, the transcript levels of Cdx2 and Eomes increased to $214.9 \pm 18\%$ and $281.0 \pm 19\%$ of control levels, respectively, whereas Gata3, another TE-marker gene, was not significantly elevated (Fig. 2c). Together, these results suggest that, in the absence of Amot, although cells can be allocated to the ICM, they express TE-specific genes and the pluripotency network (Oct4, Nanog and Sox2) becomes suppressed.

Amot acts in a cell-autonomous manner. As Amot localizes to membranes, we wondered whether it might be able to signal and affect the fate of neighbouring cells. To investigate this, we injected Amot siRNA into one blastomere at the late two-cell embryo, co-injecting Ruby mRNA as a lineage marker, and analysed embryo development at the blastocyst stage. We found that the Amot-depleted clones contributed to both inside ($53.3 \pm 1\%$) and outside ($46.7 \pm 1\%$) cells, suggesting that the cell allocation process *per se* was unaffected. In all embryos, only the clones of Amot-depleted cells were expressing Cdx2 in the ICM (Fig. 2d), suggesting that loss of Amot in one cell does not affect a neighbouring cell, and therefore Amot regulates cell fate in a cell-autonomous manner.

Amot overexpression is insufficient to drive cells to ICM. After establishing that Amot is necessary for correct ICM specification, we sought to determine whether Amot is sufficient to induce pluripotent ICM fate when overexpressed. To examine this, we injected p130-Amot mRNA into one blastomere at the late two-cell embryo, co-injecting Ruby mRNA as a marker (Fig. 2e). We confirmed Amot overexpression by immunofluorescence (Supplementary Fig. S1). Analysis of cell allocation revealed that

the Amot overexpressing clone contributed to both ICM ($46.8 \pm 2\%$) and TE ($53.2 \pm 2\%$) lineages, suggesting that Amot is insufficient to drive cells into the ICM. Interestingly, by the blastocyst stage, Amot remained highly expressed only in the ICM and markedly downregulated in the TE (Supplementary Fig. S2), pointing to a potential regulatory mechanism in the TE that degrades Amot to prevent incorrect fate specification.

Depletion of Amot with Amotl2 enhances ICM differentiation.

Our results indicate that the lack of Amot leads to the expression of differentiation genes within the ICM and downregulation of pluripotency. It has been reported that Amot^{-/-} embryos can progress beyond implantation^{18,19}, prompting us to test whether Amot-related proteins might be able to compensate for Amot function. Amot belongs to the motin family that contains two other members: Amot-like 1 (Amotl1) and Amot-like 2 (Amotl2) (Fig. 3a)²³, both of which have overlapping functions with Amot^{11-13,24}. To eliminate all three motins, we injected Amot, Amotl1, Amotl2 siRNAs into zygotes and examined developmental progression. We confirmed knockdown by qRT-PCR: Amot transcripts were depleted to $21.6 \pm 3\%$ and Amotl2 to $19.6 \pm 3\%$, whereas Amotl1 transcripts were undetectable (Fig. 3c). We found that co-depletion of Amot and Amotl2 permitted blastocyst formation (9/10, 90%; control siRNA: 9/10, 90%) and did not affect the total cell number or number of ICM cells per embryo (Fig. 3b). Strikingly, however, the proportion of Cdx2-expressing cells within the ICM was much higher in the combined motin-RNAi embryos than upon depletion of Amot alone. Nearly all ($98.0 \pm 1\%$) ICM cells of the Amot- and Amotl2-RNAi embryos were Cdx2 positive compared with the $61.8 \pm 5\%$ of Amot only-RNAi and $5.0 \pm 2\%$ of control embryos (Fig. 3b,d). This suggests that Amot and Amotl2 both function to suppress Cdx2 expression in the ICM.

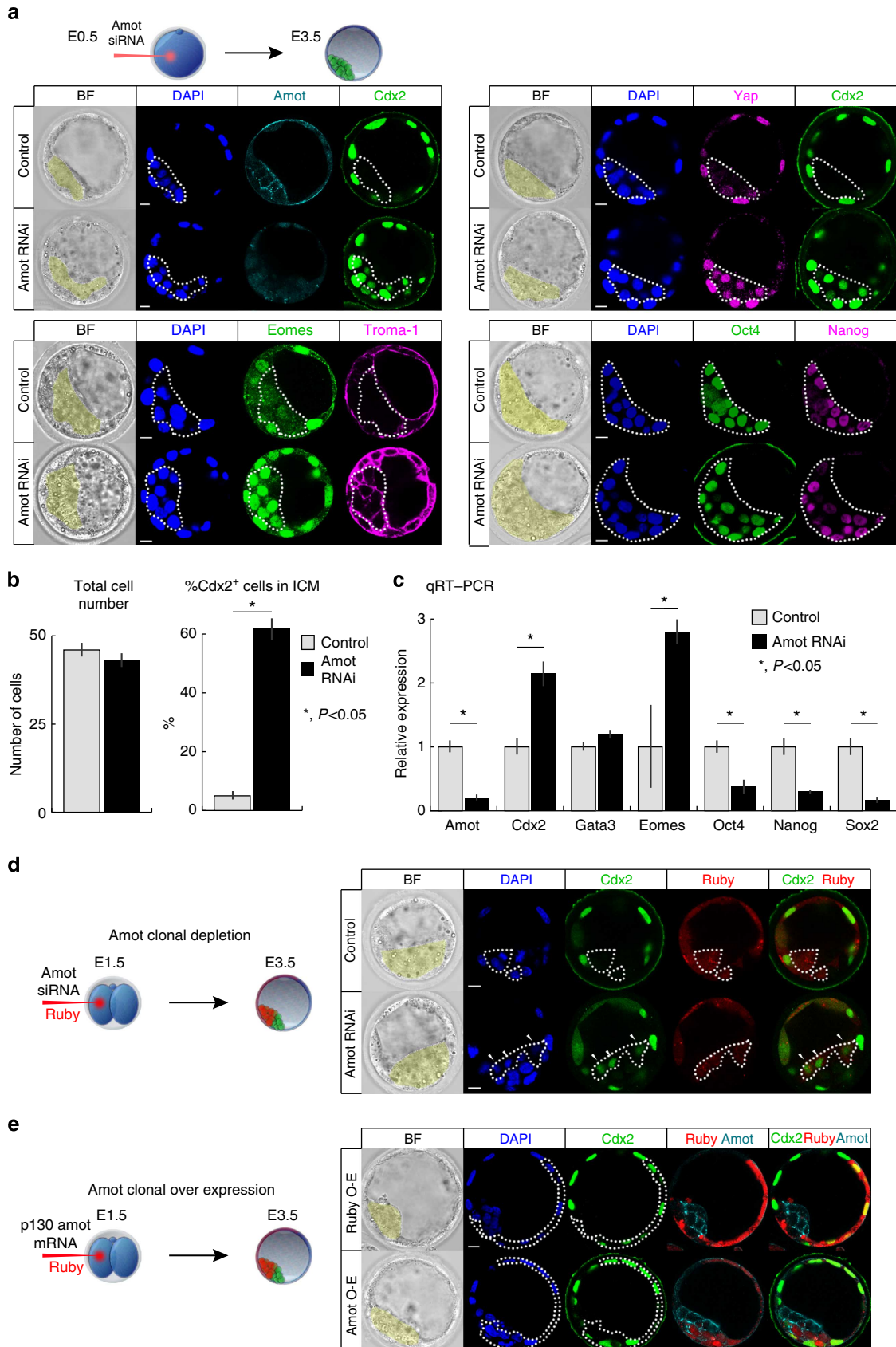
Amot depletion compromises developmental potential.

To determine whether the ICM differentiation caused by the loss of Amot would affect development *in vivo*, Amot-RNAi and Amot, Amotl1, Amotl2-RNAi embryos were transferred into pseudo-pregnant surrogates to assess their developmental potential (Supplementary Table S1). siRNAs were injected into both blastomeres at the two-cell stage, rather than the zygote, to prolong the RNAi effect (Fig. 4a). GFP transgenic embryos injected with control siRNA were used as transfer controls to normalize for transfer efficiency in different recipients. After injection, the embryos were cultured to the blastocyst stage and sampled to confirm their respective phenotypes (Fig. 4b). To assess for successful development beyond implantation, the embryos were recovered at E7.5 (Fig. 4c). After normalizing for the transfer efficiency of the different recipients and background of the embryos, we found that 100% of the control-RNAi embryos progressed successfully to E7.5, compared with 32.7% of Amot-RNAi embryos ($P < 0.05$, χ^2 -test, compared with control) and 27.8% of the combined motin-RNAi embryos ($P < 0.05$, χ^2 -test, compared with control). There was no significant difference between the developmental success of Amot-RNAi and combined motin-RNAi embryos ($P = 0.67$, χ^2 -test), although loss of all three motins might lead to a more severe outcome (Supplementary Table S2). Overall, our result suggests that loss of Amot compromises development, potentially as a result of a more differentiated ICM, signifying an important role for Amot in early mouse development.

p130-Amot is the isoform involved in cell fate regulation. The Amot protein is expressed as two isoforms, p80 and p130 (refs 21,25). The p130 isoform has a unique N-terminal extension

and the rest of the protein is identical to the p80 isoform (Fig. 5a). To determine which isoform is required for the first cell lineage specification, we depleted *Amot* with a dsRNA targeting the

3'-UTR in the zygote and then attempted to rescue *Amot*-RNAi effect with either the p80- or p130-*Amot* isoforms at the eight-cell stage. Successful knockdown by the dsRNA was confirmed by



qRT-PCR (Supplementary Fig. S3). For the rescue, we co-injected either p80- or p130-*Amot* mRNA, with Ruby mRNA as a marker, into 2–3 blastomeres at the eight-cell stage. To quantify the extent of the rescue, we determined the percentage of the Ruby- and *Cdx2*-positive cells in the ICM (Fig. 5b). In control blastocysts, $12.6 \pm 5\%$ of the Ruby-marked ICM cells were *Cdx2*-positive (Fig. 5c) (most likely owing to inherited *Cdx2* protein from an outside mother cell). This value increased significantly ($P < 0.05$, Student's *t*-test) to $88.7 \pm 4\%$ of the *Amot*-RNAi/Ruby-expressing embryos (Fig. 5c). When we injected p130-*Amot* mRNA to the *Amot*-RNAi embryos, the proportion of *Cdx2*-expressing cells in the ICM dropped significantly to $17.4 \pm 7\%$. This value was significantly different ($P < 0.05$, Student's *t*-test) from *Amot*-RNAi/Ruby-expressing embryos and not significantly different from control embryos ($P = 0.84$, Student's *t*-test), indicating that p130-*Amot* is able to fully rescue the effects of *Amot* depletion. We found that providing p80-*Amot* into *Amot*-RNAi embryos still resulted in $71.2 \pm 7\%$ of ICM cells expressing *Cdx2*, which was significantly different from the control embryos ($P < 0.05$, Student's *t*-test) (Fig. 5b,c). Therefore, the *Amot*-RNAi effect can be rescued only by the p130 isoform, indicating that p130-*Amot* function is required to suppress the differentiation pathway in the ICM.

Yap-binding motifs are involved in *Amot* function. The N-terminal extension of the p130-*Amot* contains two PPxY motifs. Mutating the tyrosine residues to alanine in the PPEY motifs abolishes the Yap-binding ability of *Amot* and its ability to tether Yap in the cytoplasm^{11–13}. A third motif conserved across all motifs, LPTY, has been suggested to mediate interaction between Yap and *Amot1* (ref. 26). These motifs therefore represent a Yap-dependent but Hippo pathway-independent activity of *Amot*. We sought to determine whether *Amot* might function in the mouse embryo independently of the Hippo pathway. We hypothesized that if overexpression of the triple motif mutant (Y110/243/288A) could rescue the *Amot*-depletion phenotype, Yap-binding motifs are consequently not important. If the opposite is true, it would follow that *Amot* functions through a Hippo pathway-independent, Yap-binding mechanism. To test this, we depleted *Amot*, from the zygote as before, and subsequently injected mRNA for Y110/243/288A *Amot* with Ruby mRNA as a lineage marker, into 2–3 blastomeres at the eight-cell stage. We found that, at the blastocyst stage, $42.0 \pm 7\%$ of the clonal Ruby-positive ICM cells were expressing *Cdx2* (Fig. 5c), which was significantly lower than that in *Amot*-RNAi embryos ($88.7 \pm 4\%$, $P < 0.05$). This suggests the Yap-binding

motifs are required for the full activity of *Amot*, and therefore *Amot* function is, in part, Yap binding dependent. In agreement with this, Yap staining in *Amot* overexpressing embryos suggests possible co-localization between Yap and *Amot* (Supplementary Fig. S4), as previously shown in MCF10A cells¹¹. In some embryos (Fig. 5c, panel v), however, *Cdx2* was not detectable in the ICM upon the Y110/243/288A mutant overexpression, suggesting that the mutant *Amot* was partially able to suppress *Cdx2* expression. Indeed, the proportion of Ruby- and *Cdx2*-positive ICM cells following injection of mRNA for Y110/243/288A *Amot* was $42.0 \pm 7\%$, an intermediate value between $17.4 \pm 7\%$ of the control and $88.7 \pm 4\%$ of the *Amot*-RNAi embryos (Fig. 5c). These results indicate that the Yap-binding sites are required for the full activity of *Amot*, raising the possibility that pluripotent lineage specification can be regulated in a Yap-binding-dependent but a Hippo pathway-independent manner.

***Amot* compensates for *Lats1/2* function.** The above results opened up a possibility that *Amot* can regulate Yap localization, and consequently *Cdx2* expression, independently of the Hippo pathway. If this is the case, *Amot* overexpression should suppress *Cdx2* expression in the absence of Hippo pathway kinases, *Lats1/2*, which phosphorylate Yap to prevent its nuclear localization⁹. To directly test this, we eliminated *Lats1* and *Lats2* transcripts by injecting zygotes with *Lats1/2* siRNAs and, at the eight-cell stage, injected 2–3 blastomeres with either Ruby mRNA only or p130-*Amot* mRNA with Ruby mRNA. We verified successful depletion of *Lats1/2* by qRT-PCR (Supplementary Fig. S5). On assessing at the morula stage, we found that *Lats1/2*-RNAi/Ruby-expressing embryos had $35.7 \pm 6\%$ of Ruby-positive inside cells expressing *Cdx2*, which was significantly more than the $5.9 \pm 4\%$ in control-RNAi/Ruby-expressing embryos of the same stage ($P < 0.05$, Student's *t*-test), in agreement with previous report⁹. Importantly, overexpression of *Amot* following *Lats1/2* depletion significantly decreased the proportion of *Cdx2*- and Ruby-positive inside cells to $18.2 \pm 4\%$ (Fig. 5c), compared with *Lats1/2*-RNAi/Ruby-expressing embryos ($P < 0.05$, Student's *t*-test). This value was not significantly different from the control-RNAi/Ruby-expressing embryos ($P = 0.06$, Student's *t*-test). These results suggest that by increasing the amount of *Amot* its Hippo pathway-independent activity can compensate for the loss of the Hippo pathway kinase *Lats1/2*.

To confirm this conclusion, we next overexpressed Y110/243/288A *Amot* that cannot bind Yap in the *Lats1/2*-RNAi background. To this end, we depleted *Lats1/2* as above, but now co-injected Y110/243/288A *Amot*, with Ruby mRNA as a lineage

Figure 2 | *Amot* prevents differentiation of the ICM. (a) Immunofluorescent confocal images of TE/ICM marker genes of control and *Amot*-RNAi blastocysts. Control ($N = 20$)/*Amot* siRNA ($N = 30$) were injected into zygotes and cultured to blastocysts; *Amot* protein was undetectable in *Amot*-RNAi blastocysts. In the absence of *Amot*, TE markers *Cdx2* ($N = 30$), *Eomes* ($N = 16$) and *Ck-8* (antibody: Troma-1) ($N = 16$) become upregulated in the ICM and Yap localized to the nuclei of ICM cells ($N = 12$) in contrast to control blastocysts, where Yap is cytoplasmic ($N = 12$). Pluripotency markers *Oct4* and *Nanog* ($N = 11$) are still visible. Yellow areas and dotted lines mark inside cells. Scale bar, 10 μm . (b) Total cell number of *Amot*-RNAi versus control blastocysts. The total number of cells between *Amot*-RNAi (46.3 ± 2 cells, $N = 20$ embryos) and control blastocysts (43.2 ± 2 cells, $N = 30$ embryos) is not significantly different ($P = 0.51$, Student's *t*-test). The percentage of *Cdx2*-positive cells in the ICM of *Amot*-RNAi blastocysts ($61.8 \pm 5\%$, $N = 434$ cells, 30 embryos) is greater than in control blastocysts ($5.0 \pm 2\%$, $N = 311$ cells, 20 embryos). Error bars represent s.e.m. Student's *t*-test was used to test significance. (c) qRT-PCR of whole embryos, comparing expression levels of several TE/ICM markers of *Amot*-RNAi ($N = 60$) versus control ($N = 60$) blastocysts. Error bars represent s.e.m. Student's *t*-test was used to test significance. (d) Immunofluorescence of embryos clonally depleted of *Amot*, showing that *Amot* governs cell fate in a cell-autonomous manner. One blastomere of two-cell embryos was injected with control/*Amot* siRNA and Ruby mRNA, and cultured to blastocysts. Ruby-positive cells mark the injected clone. In the ICM of the mosaic *Amot*-RNAi embryos, only the Ruby-positive cells expressed *Cdx2* ($N = 21$ cells) (arrows). Yellow areas mark the ICM. Dotted lines mark Ruby-positive ICM cells. Scale bar, 10 μm . (e) Immunofluorescence of embryos that are clonally overexpressing *Amot*, showing that *Amot* is not sufficient to drive cells to ICM. One blastomere of two-cell embryos was injected with Ruby mRNA only or *Amot* and Ruby mRNA, and cultured to blastocysts ($N = 10$). Ruby-positive cells mark the overexpressing clone. Yellow areas mark the ICM. Dotted lines mark Ruby-positive cells. Scale bar, 10 μm .

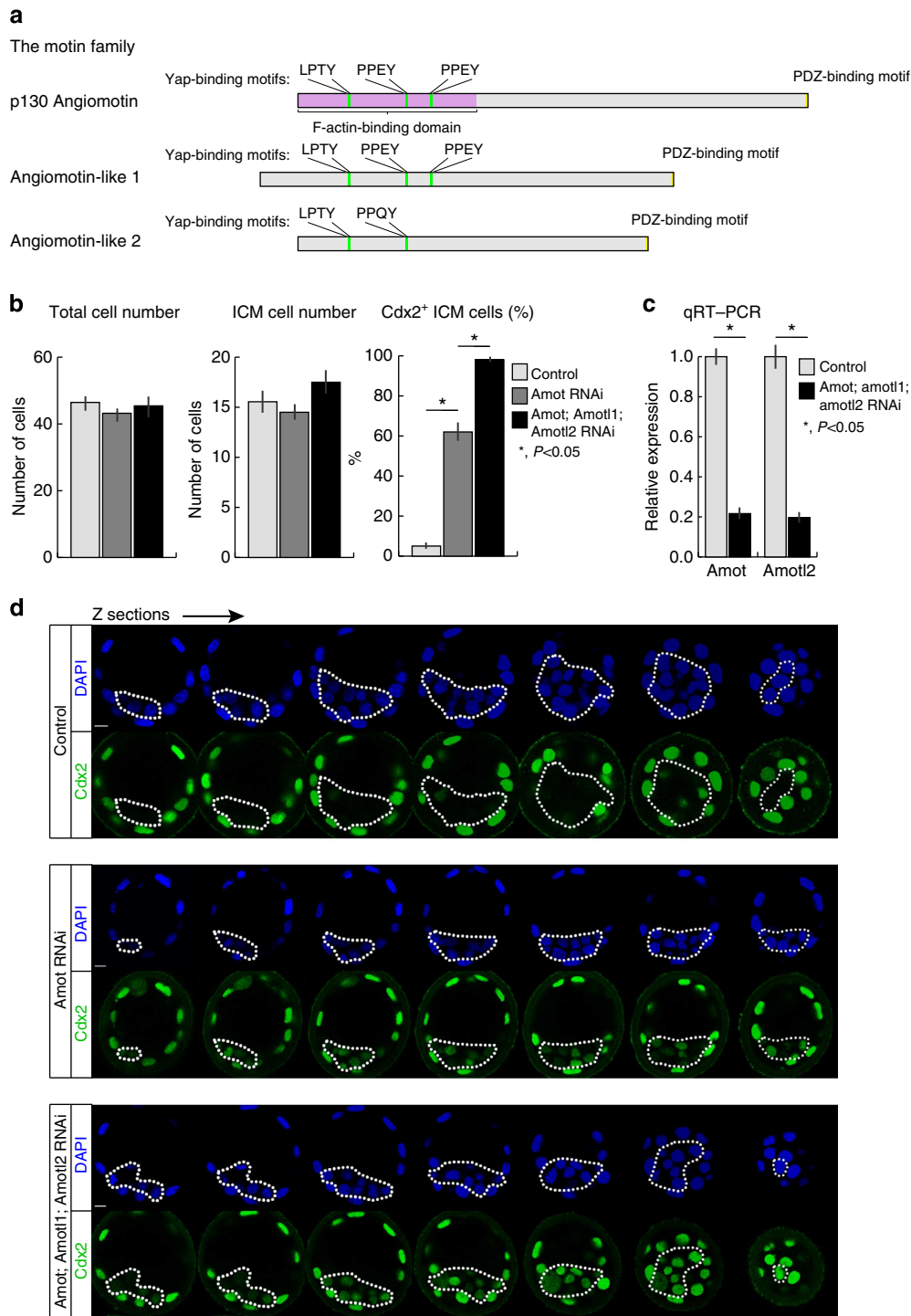


Figure 3 | Co-depletion of motin family members enhance ICM differentiation. (a) The motin family proteins with key regions outlined. (b) Total cell number and ICM cell number are not significantly different between control ($N = 21$), *Amot*-RNAi ($N = 31$) and *Amot; Amot1; Amot2*-RNAi ($N = 12$) blastocysts. However, in the triple motin-RNAi embryos, $98.0 \pm 1\%$ of ICM cells of the triple RNAi embryos were Cdx2 positive at the blastocyst stage ($N = 210$ cells, 12 embryos) compared with the $61.8 \pm 5\%$ of *Amot*-RNAi ($N = 434$ cells, 30 embryos) and $5.0 \pm 2\%$ of control embryos ($N = 311$ cells, 21 embryos). Error bars represent s.e.m. Student's *t*-test was used to test significance. (c) qRT-PCR of whole embryos, comparing expression levels of *Amot* and *Amot2* in control embryos ($N = 21$) and triple knockdown embryos ($N = 21$). *Amot* and *Amot2* were downregulated to $21.6 \pm 3\%$ and $19.6 \pm 3\%$, respectively, relative to control levels. *Amot1* expression could not be detected. Error bars represent s.e.m. Student's *t*-test was used to test significance. (d) Z-section series of immunofluorescent confocal images of control, *Amot*-RNAi ($N = 30$) and *Amot; Amot1; Amot2*-RNAi ($N = 12$) blastocysts, with the highest proportion of Cdx2-expressing cells in the triple knockdown. Dotted lines outline the ICM. Scale bar: 10 μ m.

tracer, to 2–3 blastomeres at the eight-cell stage. In these embryos, $41.4 \pm 8\%$ of the Ruby-positive inside cells were Cdx2 positive, a value not significantly different from the $35.7 \pm 6\%$ of

the *Lats1/2*-RNAi/Ruby-expressing embryos ($P = 0.58$, Student's *t*-test) (Fig. 5c). Thus, the Y110/243/288A mutant is not able to compensate for the loss of *Lats1/2*, further pointing to a direct

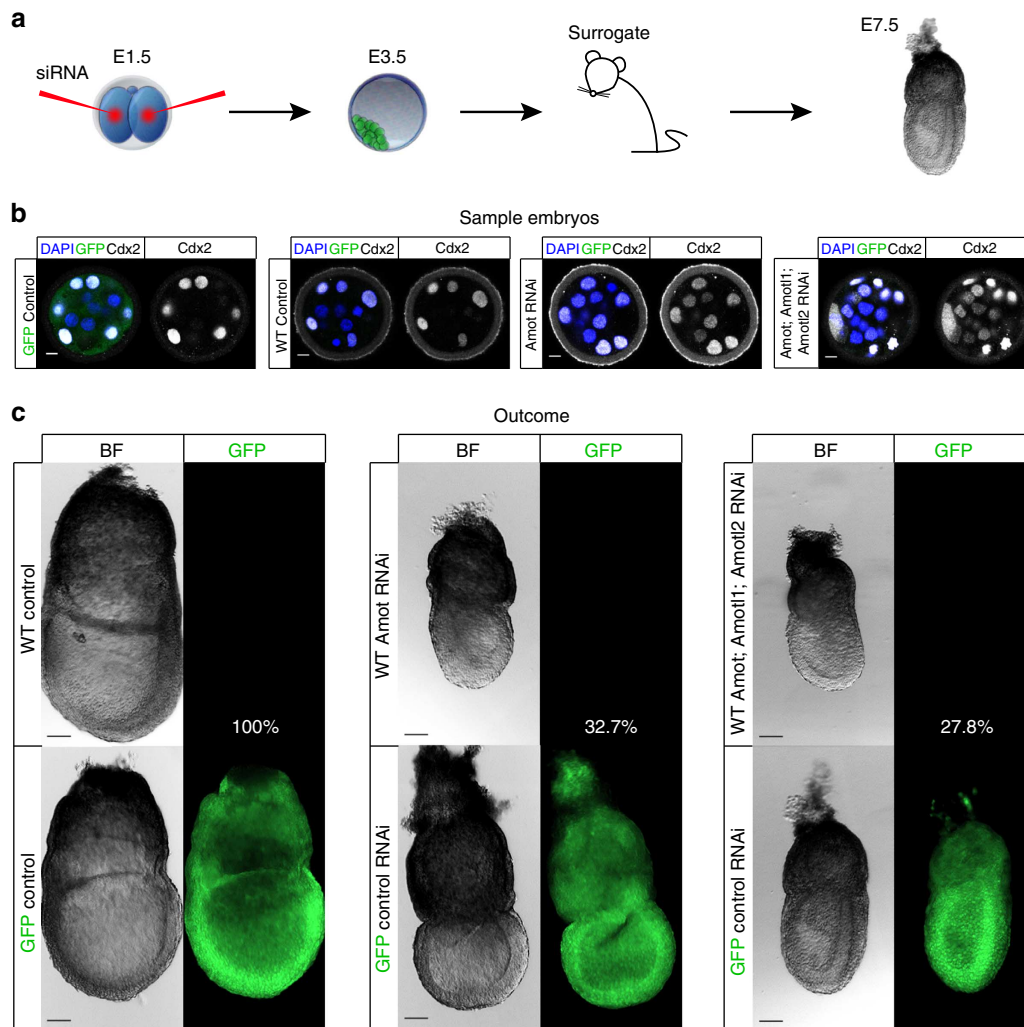


Figure 4 | Loss of AMOT compromises the developmental potential of peri-implantation embryos. (a) Experimental outline: siRNA was injected to both blastomeres of two-cell-stage embryo, cultured to E3.5 and transferred to 2.5 dpc pseudo-pregnant recipients. The embryos were recovered 5 days later at E7.5. Embryos were injected with either control siRNA, *Amot* siRNA or a combination of *Amot*, *Amotl1* and *Amotl2* siRNA. For each of the three groups (control, *Amot*-RNAi and *Amot*; *Amotl1*; *Amotl2*-RNAi), 20 WT embryos and 20 GFP embryos were transferred to two surrogates. (b) Embryos from each group were sampled to confirm their phenotype following RNAi. *Amot*-RNAi embryos ($N = 9$) and *Amot*; *Amotl1*; *Amotl2*-RNAi ($N = 6$) expressed CDX2 in the inside cells, whereas in GFP ($N = 10$) and WT ($N = 10$) embryos injected with control siRNA CDX2 expression was restricted to the outside cells. (c) The outcome of the embryo transfers. To assess for developmental success, the embryos were recovered at E7.5. For the control-RNAi group, out of the 40 embryos transferred, 38 embryos were recovered, of those 20 (100%) were GFP+ and 18 (90%) were GFP-. For *Amot*-RNAi, out of 40 embryos transferred, 22 embryos were recovered, of those 17 (85%) were GFP+ and 5 (25%) were GFP-. For the *Amot*; *Amotl1*; *Amotl2*-RNAi, out of 40 embryos transferred, 20 embryos were recovered, of those 16 (80%) were GFP+ and 4 (20%) were GFP-. After normalizing for the transfer efficiency of the different recipients and background of the embryos, 100% of the control-RNAi embryos progressed successfully to E7.5, compared with 32.7% of *Amot*-RNAi embryos ($P < 0.05$, χ^2 -test, compared with control) and 27.8% of *Amot*; *Amotl1*; *Amotl2*-RNAi embryos ($P < 0.05$, χ^2 -test, compared with control). There was no significant difference between the developmental success of *Amot*-RNAi and *Amot*; *Amotl1*; *Amotl2*-RNAi embryos ($P = 0.67$, χ^2 -test). Scale bar, 100 μ m.

Amot/Yap interaction that bypasses the classical Hippo pathway. On a side note, this also indicates that the *Lats1/2* phenotype is Yap dependent, as only *Amot* with intact Yap-binding sites can compensate for *Lats1/2* function. Taken together, these results further indicate that *Amot* can function in a Yap-dependent but Hippo pathway-independent manner to specify cell fate in the mouse embryo.

Discussion

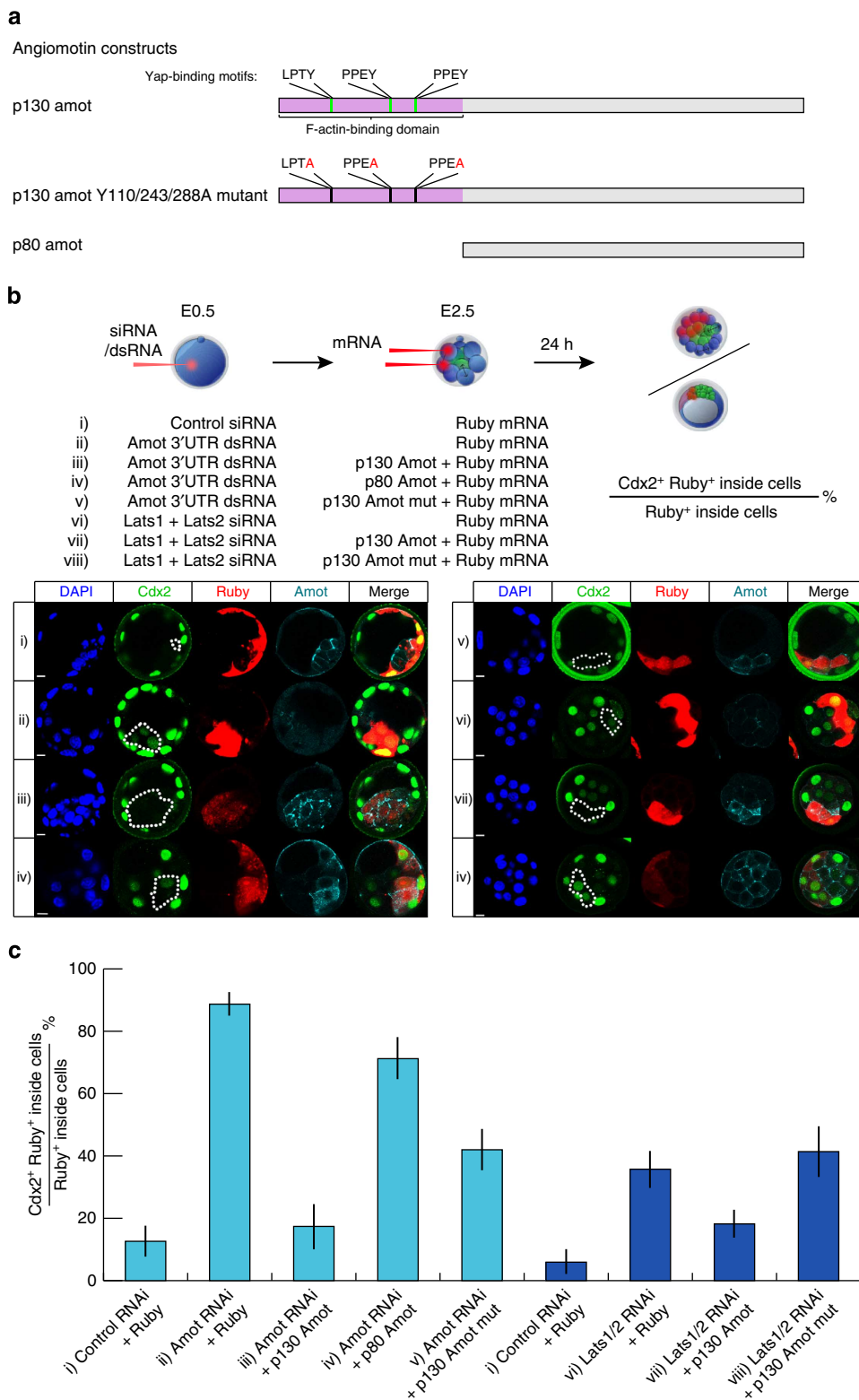
Analyses of spatial and temporal expression patterns together with the downregulation and overexpression studies we present

here identify *Amot* as a new important regulator of the first cell fate specification in the mouse embryo. We find that *Amot* becomes enriched in the ICM versus TE progenitor cells as development progresses; *Amot* is critical to prevent expression of TE-marker genes in the pluripotent lineage; ICM differentiation is significantly enhanced by co-depletion of *Amot* with *Amotl2*; *Amot* regulates localization of Yap; full activity of *Amot* is dependent on the Yap-binding motifs, suggesting a Hippo pathway-independent function; *Amot* function can compensate for the absence of *Lats1/2*, supporting its ability to function independently of the Hippo pathway; and mutating the Yap-binding motifs affects, but does not completely abolish, *Amot*

activity, suggesting that Amot might also act through an alternative mechanism, such as through activating Lats1/2 via the Hippo pathway or independent of Yap and, finally, that Amot depletion, together with depletion of Amotl2, results in compromised development at peri-implantation stages. Overall, our results identify a role of Amot in the first-lineage specification to prevent an inappropriate cell fate program in the

pluripotent ICM and suggest that Amot has two distinct roles in this process, sequestering Yap, which is Hippo pathway independent, and also activating the Hippo pathway kinase Lats1/2 (Fig. 6).

Our results indicate that loss of Amot results in the upregulation of genes that promote differentiation and, consequently, downregulation of pluripotency genes such as *Oct4*,



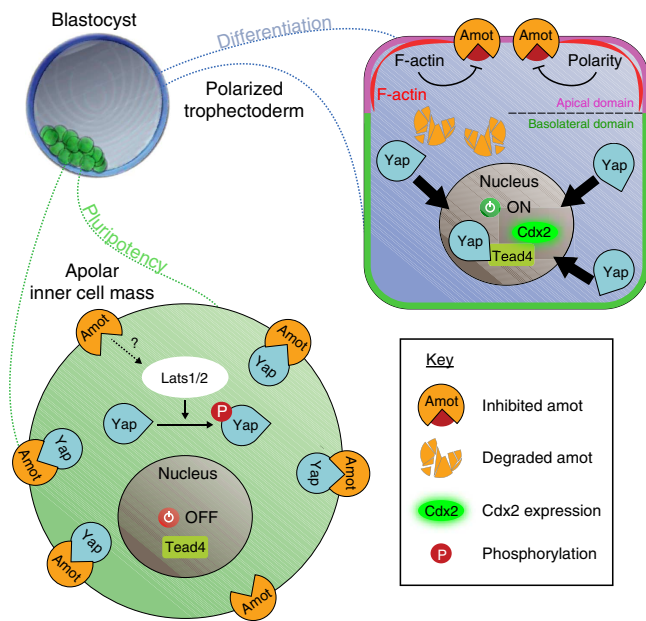


Figure 6 | Hippo pathway-dependent and -independent mechanisms in lineage segregation. The results we present here show that Amot becomes enriched in the ICM as cell lineages become progressively established, and that Amot functions to prevent differentiation of the pluripotent lineage. Our results suggest that Amot acts through two routes to prevent ICM differentiation, of which one is dependent and another is independent of the Hippo pathway. The Hippo pathway-independent (Lats1/2-independent) mechanism is likely to involve Amot’s ability to tether Yap to the cytoplasm/membrane, as we find that Yap-binding motifs of Amot are essential for its full activity. But, it can also involve Amot interacting with actin/cell polarity molecules. The Hippo pathway-dependent mechanism is likely to involve Amot’s role in activating Lats1/2 (as shown in²⁴) to allow phosphorylation of Yap, which prevents its transition to the nucleus⁹. In agreement, we find that mutation of the Yap-binding sites does not completely abolish the activity of Amot. Combined, this results in Yap being sequestered from the nucleus and therefore the expression of TE-genes, such as Cdx2, is switched off and the ICM pluripotency maintained. In contrast, in TE cells, most of Amot is degraded and the remaining Amot is sequestered to the apical domain. We hypothesize that in this location Amot is shielded from binding Yap through its interactions with F-actin and/or polarity factors. In agreement with this hypothesis, Amot is reported to associate with actin³² and tight-junction proteins via its PDZ-binding domain in tissue culture cells^{14–17}. This suggests that cell polarity is involved in allowing Yap to translocate to the nucleus to act, together with Tead4, to stimulate Cdx2 expression and TE differentiation.

Nanog and *Sox2* in the ICM. Despite this, we observe that some pluripotency-associated transcription factors are still present, possibly as a result of pre-existing protein. This finding is likely to explain why *Amot*^{-/-} embryos can survive through implantation and arrest only at early post-implantation stages^{18,19}. This could also be due to developmental plasticity, as the mouse embryo has been shown to require establishment of only four pluripotent cells by implantation to support its development to birth⁴. Finally, genetic redundancy could also be a contributing factor, as we show here that simultaneous depletion of *Amot* and *Amot2* lead to a much stronger phenotype than depletion of *Amot* on its own.

As development progresses, *Amot* becomes upregulated in ICM but not TE progenitors. A deep sequencing analysis of global gene expression patterns between ICM and TE progenitors after the first wave of asymmetric division, at the 16-cell stage, reveals similar levels of *Amot* mRNA (Krzysztof Wicher, Sarah Graham and Magdalena Zernicka-Goetz, unpublished observations). Although this does not rule out differential transcription later, our results suggest that *Amot* enrichment in the ICM might result from differential stability of the protein between ICM and TE cells. In support of this, we show that when *Amot* is overexpressed, it is downregulated in TE but not in ICM cells (Supplementary Fig. S2). Moreover, one of the E3 ubiquitin ligases able to promote *Amot* degradation²⁷, NEDD4L, is expressed two-fold higher in TE than in ICM progenitors (Krzysztof Wicher, Sarah Graham and Magdalena Zernicka-Goetz, unpublished observations), thus giving the potential of reducing *Amot* levels in TE. In addition, cytoplasmic Yap has been found to protect *Amot1* from NEDD4-mediated degradation²⁶, raising an interesting possibility that Yap could act in a positive feedback loop to prevent *Amot* degradation in the ICM.

Two models are often considered for the first cell fate decision in the mouse embryo. The polarity model¹ stresses the importance of cell polarity in directing cell fate, and the positional model^{28,29} stresses the importance of cell position. It has been demonstrated that cell polarity and cell position re-enforce each other³⁰, and these two models can be brought together conceptually³¹. Identifying *Amot* as a cell fate regulator is a molecular step towards this unification, because it lends support to both: *Amot* becomes enriched in inside but not outside cells (supporting a positional ‘inside-outside’ model) and its localization is polarized in outside cells (supporting a ‘polarity’ model). Apically localized *Amot* in polarized outside cells may interact with polarity factors, and, in support of this idea, it has been already shown to associate with tight-junction proteins via its PDZ-binding domain^{14–17}. Therefore, we would like to suggest that, in the mouse embryo, as in other model systems, cell polarity is involved in Yap regulation as it can, for example,

Figure 5 | p130-Amot functions independently of the Hippo pathway kinases Lats1/2. (a) Amot constructs with key regions outlined. The p80- and p130-Amot isoforms are identical, except the p130 isoform has an N-terminal extension, which contains three Yap-binding motifs. (b) Eight sets of experiments (i)–(viii) are shown, which follow the same experimental outline: siRNA/dsRNA was injected into the zygote and mRNA was injected into two or three blastomeres at the eight-cell stage. Cdx2-positive inside cells from all eight sets of experiments were counted manually. The phenotype was quantified by the percentage of Cdx2-positive cells from the Ruby-positive inside cells at the blastocyst stage (or the morula stage in the case of *Lats1/2* knockdown). Panels show confocal images of representative embryos from each set of experiments. Dotted lines mark Ruby-positive inside cells. Scale bar, 10 μm. (c) Combined quantifications from the experiments outlined in (b). Number of biological replicates: (i) N = 41 cells, 15 embryos; (ii) N = 96 cells, 34 embryos; (iii) N = 53 cells, 35 embryos; (iv) N = 44 cells, 11 embryos; (v) N = 20 cells, 40 embryos; (vi) N = 22 cells, 9 embryos; (vii) N = 139 cells, 24 embryos; (viii) N = 145 cells, 43 embryos; (viii) N = 58 cells, 18 embryos. Error bars represent s.e.m. This quantification shows that the p130, but not the p80, isoform is able to rescue the *Amot* phenotype and the Yap-binding motifs are required for the full activity of p130-Amot. *Lats1/2* depletion leads to an increased Cdx2-positive inside cell number, but overexpression of p130-Amot is able to prevent Cdx2 expression in the absence of *Lats1/2*, demonstrating a Hippo pathway-independent mechanism. Confirming this conclusion overexpressing the *Amot* mutant for Yap-binding motifs in a *Lats1/2*-RNAi background does not affect the *Lats1/2* phenotype.

inhibit Amot's ability to bind Yap to restrain its translocation to the nucleus (Fig. 6).

The ability of Amot to function through Yap is strongly suggested by the three putative Yap-binding motifs of p130-Amot that are absent in p80-Amot and which we show here are essential for the full activity of Amot. Indeed, Yap seemingly co-localizes with p130-Amot when p130-Amot is overexpressed (Supplementary Fig. S4). Another way to test Amot's Yap dependence would be through an *Amot*; *Yap* double knockdown. However, interpreting such an experiment would be difficult because of the redundancy of Yap with its homologue *Taz*⁹ (Supplementary Fig. S6).

We find that Amot is partly functional following mutation of its Yap-binding sites, which suggests that two possible mechanisms of Amot function are tenable. One would reflect the direct interaction between Amot and Yap, independent of the Hippo pathway. The second would reflect the residual function of this Yap-binding defective Amot mutant that would still be able to activate Lats1/2, leading to Yap phosphorylation and cytoplasmic retention (as demonstrated in HEK293 cells²⁴). Our results cannot also rule out the possibility that the residual function of this Amot mutant reflects function that is entirely independent of Yap.

The key regulatory domain of Amot appears to be its N-terminal part, as we show that the p80 isoform does not have a role in cell fate regulation. This N-terminal domain could be responsible for activation of Lats1/2-dependent phosphorylation of Yap, as supported by *in vitro* data²⁴. We also consider the actin-binding properties of the N-terminal domain of p130-Amot³² could relate to its ability to suppress *Cdx2* expression in the pluripotent lineage. In agreement with this hypothesis, it has been reported that an increase in filamentous actin results in increased nuclear Yap and activation of Yap target genes^{33–38}. Finally, we show that overexpressing p130-Amot prevents the expression of *Cdx2* in inside cells lacking Lats1/2. Hence, in the absence of the Hippo pathway, high levels of Amot are sufficient to sequester most of the Yap molecules from the nucleus. Taken together, our results suggest that both Hippo pathway-dependent and -independent processes are involved in regulating Yap localization to generate pluripotent cells in the mouse embryo.

Methods

Embryo collection and culture. Animals were maintained in the Animal Facility of Gurdon Institute at 12:12 light cycle and provided with food and water *ad libitum*. All experiments were conducted in compliance with Home Office regulations. For embryo collection, 4- to 6-week-old F₁ generation mice from the C57Bl6 and CBA strains were superovulated with 10 IU of pregnant mare serum gonadotropin (PMSG; Intervet) and 10 IU human chorionic gonadotropin (hCG; Intervet) 48 h later and mated with F₁ (C57Bl6 × CBA) male mice. Embryos were dissected out of the oviducts into M2 medium. For zygote recovery, cumulus cells were removed by hyaluronidase treatment (1 mg ml⁻¹ in M2). Embryos were cultured in drops of KSOM media (Millipore) under paraffin oil in 5% CO₂ at 37 °C.

Immunohistochemistry and analysis. Embryos were fixed in 4% PFA for 20 min and washed twice for 5 min in PBS-T (PBS with 0.1% Tween). They were then permeabilized with 0.5% Triton X-100 in PBS for 20 min and washed three times for 5 min in PBS-T. The embryos were incubated with primary antibodies diluted in 3% BSA (Sigma) for 1 h. *Cdx2* antibody (Biogenex) was used at a dilution of 1:200; Oct4 antibody (Santa Cruz) at 1:200; Nanog antibody (2BSscientific) at 1:200; Yap antibody (Santa Cruz) at 1:400; Eomes antibody (Abcam) at 1:250; Troma-1 at 1:100; and Amot antibody (Santa Cruz) at 1:2,000. The embryos were then washed three times for 5 min in PBS-T. Secondary antibodies (Invitrogen, AlexaFluor) and DAPI (Invitrogen) were applied for 1 h at a dilution of 1:400 in 3% BSA (Sigma). After washing three times for 5 min in PBS-T, the embryos were washed overnight in M2 medium. Embryos were imaged on glass-bottom dishes rather than on slides in order to avoid flattening the embryo. Confocal images were captured with a Leica SP5 confocal microscope with a Z-resolution of 4 μm. All images are layer-normalized using IMARIS to account for signal intensity differences from different sections. To count total cell numbers, DAPI was used as a nuclear marker to represent each cell. Acquisition of *Cdx2* stainings for cell counting was performed

using identical settings on a Leica SP5. To count *Cdx2*-positive cells, the confocal z-stacks were first exported to IMARIS and layer-normalized using the built-in function. The normalized sections were then assessed for the presence of *Cdx2* signal. Any nuclei with signal detectable by eye were scored as 'Cdx2 positive'. Cells were then manually counted in ImageJ using the MTrackJ plug-in. Student's *t*-test, unless otherwise stated, was used to test statistical significance.

RNAi reagents and construct preparation. p130- and p80-*Amot* were cloned from mouse kidney cDNA and sequence verified. mRNA was synthesized using the mMESSAGE mMACHINE Kit (Life Technologies). dsRNA was designed and evaluated using E-RNAi, a web application for the design of RNAi reagents³⁹. The DNA template of the dsRNA was amplified from mouse kidney cDNA, and dsRNA was synthesized from DNA using the T7 MEGAscript kit (Life Technologies). The dsRNA was annealed by heating to 70 °C for 5 min and allowed to cool at room temperature for 2 h. It was treated with RNase T1/A and Proteinase K to remove ssRNA and proteins. Site-directed mutagenesis of the PPxY motifs was performed via overlap extension PCR. Four PCR fragments were amplified from *Amot* DNA using mutagenic primers, with two fragments overlapping over each PPxY motif. All four fragments were pooled, annealed and PCR amplified into one complete piece of DNA, which was sequence verified. The following is the sequence of *Amot* siRNA used: 5'-CAGGAGAAGCCTACTCA GCTA-3'. Primers used for cloning are as follows: p80-*Amot* 5'-TTTTGGAT CCACCATGCCTCGGGCTCAG-3' 5'-TTCGTTTTCGGCCGCTTAGATGAGA TATTCC-3'; p130-*Amot* 5'-TTTTTTTTTTGGATCCACCATGAGAAGTTCT CACGATCAGCC-3' 5'-TTTTTTTTTTTCGGCCGCTTAGATGAGATATTC GACC-3'. The following primers were used to generate the p130-*Amot* Y110/243/288A mutant: 5'-TTTTTTTTTTGGATCCACCATGAGAAGTTCTG ACGATCAGCC-3'; 5'-GACCTTGGCCTCTTCGGCCGTTGGGAGTTCTTC-3'; 5'-GAAGAAGTCCCAACCGCCGAAGAGGCCAAGGTC-3'; 5'-TTTTTTTTTT ATGCATCCTTCTAATCTCGCCCTCCAGCTTGTTC-3'; 5'-CCCTTGAAGG GGCTTCTGGCGGGGACCTC-3'; 5'-GAGGTCCCCCGCCAGAAGCCCTTT CAAGG-3'; 5'-CTGCCCGCCTCAGGGGGTGTCTGATA-3'; 5'-TATCAG CACCCCTTGAGGCCGGGCGAG-3'. The following primers were used to generate dsRNA targeting the 3'-UTR of *Amot*: 5'-TAATACGACTCACTATAGG GTGTGTTTGGGGAGAAAAGGA-3'; 5'-TAATACGACTCACTATAGGGAAG TCCAGGAAAAGGCCTGA-3'.

Embryo microinjection. Microinjection was performed on a Leica DM IRB with attached Leica micromanipulators. Injections were administered via air pressure using an Eppendorf Femtojet microinjector, and negative capacitance was used to facilitate membrane penetration. All injections were carried out on embryos suspended in M2 medium under paraffin oil on a depression slide. Successful microinjections were confirmed by the presence of fluorescent markers co-injected with the constructs. Ruby mRNA (0.4 mg ml⁻¹) was co-injected for all experiments except in the rescue experiments where 0.4 mg ml⁻¹ Gap-RFP was co-injected to mark the membrane without interfering with the cytoplasmic Ruby introduced at the eight-cell stage.

qRT-PCR. RNA was extracted from embryos using the Arcturus PicoPure RNA Isolation Kit. qRT-PCR was carried out using SYBR Green in a StepOne Plus Real-time PCR machine (Applied Biosystems). *Gapdh* was used as an endogenous control. The following primers were used: *Gapdh* 5'-AGAGCGCCGCATC TTC-3' 5'-CCCAATACGGCCAAATCCGT-3'; *Amot* 5'-GATGTGCAACCCAGA TAAGCC-3' 5'-TCTCTGCATCAGGCTCTTGC-3'; *Cdx2* 5'-AAACCTGTGCGA GTGGATG-3' 5'-TCTGTGTACACCACCCGGTA-3'; *Eomes* 5'-CGGCCATCCA AAACACGGAT-3' 5'-AAGCCGTGTACATCGAATCGTA-3'; *Gata3* 5'-CCGA AACCGGAAGATGTCTA-3' 5'-AGATGTGGCTCAGGGATGAC-3'; *Oct4* 5'-TT GGGCTAGAGAAGGATGTGGTT-3' 5'-GGAAAAGGGACTGAGTAGAGTGTG G-3'; *Nanog* 5'-GGTGAAGACTAGCAATGGTTCTGA-3' 5'-TGCAATGGAT GCTGGGATACTC-3'; *Sox2* 5'-TGCTGCCTCTTTAAGACTAGGG-3' 5'-CGCC GCGATTGTTGTGATT-3'; *Lats1* 5'-AACAGTTCTCCGGAGCC-3' 5'-ACC ATGTCTCATCAAAGCCA-3'; *Lats2* 5'-GAATCGGGATGTGACCAG-3' 5'-TACTCCAAGGCAGCTTCGAT-3'.

References

- Johnson, M. H. & Ziomek, C. A. The foundation of two distinct cell lineages within the mouse morula. *Cell* **24**, 71–80 (1981).
- Bruce, A. W. & Zernicka-Goetz, M. Developmental control of the early mammalian embryo: competition among heterogeneous cells that biases cell fate. *Curr. Opin. Genet. Dev.* **20**, 485–491 (2010).
- Morris, S. A., Teo, R. T. Y., Li, H., Robson, P., Glover, D. M. & Zernicka-Goetz, M. Origin and formation of the first two distinct cell types of the inner cell mass in the mouse embryo. *Proc. Natl. Acad. Sci. USA* **107**, 6364 (2010).
- Morris, S. A., Guo, Y. & Zernicka-Goetz, M. Developmental plasticity is bound by pluripotency and the Fgf and Wnt signaling pathways. *Cell Rep.* **2**, 756–765 (2012).
- Strumpf, D. *et al.* *Cdx2* is required for correct cell fate specification and differentiation of trophoblast in the mouse blastocyst. *Development* **132**, 2093–2102 (2005).

6. Jedrusik, A. *et al.* Role of Cdx2 and cell polarity in cell allocation and specification of trophoblast and inner cell mass in the mouse embryo. *Genes Dev.* **22**, 2692–2706 (2008).
7. Jedrusik, A. *et al.* Maternally and zygotically provided Cdx2 have novel and critical roles for early development of the mouse embryo. *Dev. Biol.* **344**, 66–78 (2010).
8. Skamagki, M., Wicher, K. B., Jedrusik, A., Ganguly, S. & Zernicka-Goetz, M. Asymmetric localization of Cdx2 mRNA during the first cell-fate decision in early mouse development. *Cell. Rep.* **3**, 442–457 (2013).
9. Nishioka, N. *et al.* The Hippo signaling pathway components Lats and Yap pattern Tead4 activity to distinguish mouse trophoblast from inner cell mass. *Dev. Cell* **16**, 398–410 (2009).
10. Genevet, A. & Tapon, N. The Hippo pathway and apico-basal cell polarity. *Biochem. J.* **436**, 213–224 (2011).
11. Zhao, B. *et al.* Angiominin is a novel Hippo pathway component that inhibits Yap oncoprotein. *Genes Dev.* **25**, 51–63 (2011).
12. Wang, W., Huang, J. & Chen, J. Angiominin-like proteins associate with and negatively regulate Yap1. *J. Biol. Chem.* **286**, 4364–4370 (2011).
13. Chan, S. W., Lim, C. J., Chong, Y. F., Pobbati, A. V., Huang, C. & Hong, W. Hippo pathway-independent restriction of TAZ and Yap by angiominin. *J. Biol. Chem.* **286**, 7018–7026 (2011).
14. Sugihara-Mizuno, Y. *et al.* Molecular characterization of angiominin/JEAP family proteins: interaction with MUPP1/Patj and their endogenous properties. *Genes Cells* **12**, 473–486 (2007).
15. Wells, C. D. *et al.* A Rich1/Amot complex regulates the Cdc42 GTPase and apical-polarity proteins in epithelial cells. *Cell* **125**, 535–548 (2006).
16. Ernkvist, M. *et al.* The Amot/Patj/Syx signaling complex spatially controls RhoA GTPase activity in migrating endothelial cells. *Blood* **113**, 244–253 (2009).
17. Yi, C. *et al.* A tight junction-associated Merlin-angiominin complex mediates Merlin's regulation of mitogenic signaling and tumor suppressive functions. *Cancer Cell* **19**, 527–540 (2011).
18. Shimono, A. & Behringer, R. R. Angiominin regulates visceral endoderm movements during mouse embryogenesis. *Curr. Biol.* **13**, 613–617 (2003).
19. Aase, K. *et al.* Angiominin regulates endothelial cell migration during embryonic angiogenesis. *Genes Dev.* **21**, 2055–2068 (2007).
20. Wang, Q. T. *et al.* A genome-wide study of gene activity reveals developmental signaling pathways in the preimplantation mouse embryo. *Dev. Cell* **6**, 133–144 (2004).
21. Bratt, A. *et al.* Angiominin regulates endothelial cell-cell junctions and cell motility. *J. Biol. Chem.* **280**, 34859–34869 (2005).
22. Wianny, F. & Zernicka-Goetz, M. Specific interference with gene function by double-stranded RNA in early mouse development. *Nat. Cell Biol.* **2**, 70–75 (2000).
23. Bratt, A. *et al.* Angiominin belongs to a novel protein family with conserved coiled-coil and PDZ binding domains. *Gene* **298**, 69–77 (2002).
24. Paramasivam, M., Sarkeshik, A., Yates, 3rd J. R., Fernandes, M. J. G. & McCollum, D. Angiominin family proteins are novel activators of the Lats2 kinase tumor suppressor. *Mol. Biol. Cell* **22**, 3725–3733 (2011).
25. Ji, W. R. *et al.* Characterization of kringle domains of angiostatin as antagonists of endothelial cell migration, an important process in angiogenesis. *FASEB J* **12**, 1731–1738 (1998).
26. Skouloudaki, K. & Walz, G. Yap1 recruits c-Abl to protect angiominin-like 1 from Nedd4-mediated degradation. *PLoS One* **7**, e35735 (2012).
27. Wang, C. *et al.* The Nedd4-like ubiquitin E3 ligases target angiominin/p130 to ubiquitin-dependent degradation. *Biochem. J.* **444**, 279–289 (2012).
28. Hillman, N., Sherman, M. I. & Graham, C. The effect of spatial arrangement on cell determination during mouse development. *J. Embryol. Exp. Morphol.* **28**, 263–278 (1972).
29. Tarkowski, A. K. & Wróblewska, J. Development of blastomeres of mouse eggs isolated at the 4- and 8-cell stage. *J. Embryol. Exp. Morphol.* **18**, 155–180 (1967).
30. Plusa, B. *et al.* Downregulation of Par3 and aPKC function directs cells towards the ICM in the preimplantation mouse embryo. *J. Cell. Sci.* **118**, 505 (2005).
31. Zernicka-Goetz, M., Morris, S. A. & Bruce, A. W. Making a firm decision: multifaceted regulation of cell fate in the early mouse embryo. *Nat. Rev. Genet.* **10**, 467–477 (2009).
32. Ernkvist, M. *et al.* p130-angiominin associates to actin and controls endothelial cell shape. *FEBS J.* **273**, 2000–2011 (2006).
33. Dupont, S. *et al.* Role of Yap/TAZ in mechanotransduction. *Nature* **474**, 179–183 (2011).
34. Fernández, B. G., Gaspar, P., Brás-Pereira, C., Jezowska, B., Rebelo, S. R. & Janody, F. Actin-capping protein and the hippo pathway regulate F-actin and tissue growth in Drosophila. *Development* **138**, 2337–2346 (2011).
35. Sansores-Garcia, L. *et al.* Modulating F-actin organization induces organ growth by affecting the Hippo pathway. *EMBO J.* **30**, 2325–2335 (2011).
36. Visser-Grieve, S. *et al.* Lats1 tumor suppressor is a novel actin-binding protein and negative regulator of actin polymerization. *Cell Res.* **21**, 1513–1516 (2011).
37. Wada, K.-I., Itoga, K., Okano, T., Yonemura, S. & Sasaki, H. Hippo pathway regulation by cell morphology and stress fibers. *Development* **138**, 3907–3914 (2011).
38. Zhao, B., Li, L., Wang, L., Wang, C.-Y., Yu, J. & Guan, K.-L. Cell detachment activates the Hippo pathway via cytoskeleton reorganization to induce anoikis. *Genes Dev.* **26**, 54–68 (2012).
39. Horn, T. & Boutros, M. E-RNAi: a web application for the multi-species design of RNAi reagents—2010 update. *Nucleic Acids. Res.* **38**, W332–W339 (2010).

Acknowledgements

We thank W. Mansfield for assistance on the embryo transfer experiments and our colleagues for advice and to the Wellcome Trust for funding.

Author contributions

All experiments were performed in M.Z.G.'s laboratory by C.Y.L. The data were analysed and interpreted by C.Y.L. and M.Z.G. The manuscript was written by C.Y.L. and M.Z.G.

Additional information

Supplementary Information accompanies this paper at <http://www.nature.com/naturecommunications>

Competing financial interests: The authors declare no competing financial interests.

Reprints and permission information is available online at <http://npg.nature.com/reprintsandpermissions/>

How to cite this article: Leung, C.Y. and Zernicka-Goetz M. Angiominin prevents pluripotent lineage differentiation in mouse embryos via Hippo pathway-dependent and independent mechanisms. *Nat. Commun.* **4**:2251 doi: 10.1038/ncomms3251 (2013).



This article is licensed under a Creative Commons Attribution 3.0 Unported Licence. To view a copy of this licence visit <http://creativecommons.org/licenses/by/3.0/>.